A mathematical model for predicting the temperature distribution in laser-induced hyperthermia. Experimental evaluation and applications

Sturesson, C; Andersson-Engels, Stefan

Published in:
Physics in Medicine and Biology

DOI:
10.1088/0031-9155/40/12/003

1995

A mathematical model for predicting the temperature distribution in laser-induced hyperthermia. Experimental evaluation and applications

1995 Phys. Med. Biol. 40 2037

(http://iopscience.iop.org/0031-9155/40/12/003)

Phys. Med. Biol. 40 (1995) 2037–2052. Printed in the UK

A mathematical model for predicting the temperature distribution in laser-induced hyperthermia. Experimental evaluation and applications

C Sturesson and S Andersson-Engels
Department of Physics, Lund Institute of Technology, PO Box 118, S-22 100 Lund, Sweden

Received 9 March 1995, in final form 3 August 1995

Abstract. A time-dependent mathematical model for the heat transfer in laser-induced hyperthermia has been developed. The model calculates the temperature distribution in surface-irradiated tissues. Good agreement was found between the predictions of the model and *in vitro* experimental results obtained for bovine liver irradiated with an expanded beam from a Nd:YAG laser. Surface evaporation of water was included in the model and experimentally verified. The discrepancy between the measured and the calculated rise in temperature at three different depths on the axis of symmetry of the irradiating beam was found to be less than 5% after 15 min of irradiation. When irradiating in air and not accounting for the surface evaporation in the model, the accuracy of the model predictions was only 75–80%. The model was then used to investigate the influence of surface evaporation of water on the total temperature distribution theoretically in a clinically relevant case. From the numerical simulations, it was shown that, simply by providing a moistened liver surface, the maximum steady-state temperature could be forced into the tissue to a depth of 4 mm. It was also shown that, by employing the numerical model during the initial phase of hyperthermia treatment, overshooting of the temperature during the transient thermal build-up time could be prevented.

1. Introduction

The potential of hyperthermia as a cancer treatment modality, used either as a single agent or in combination with radiation or chemotherapy, has been recognized by many investigators (for reviews, see Overgaard 1989, Molls 1992 and Seegenschmiedt *et al* 1993). In recent years, the combination of hyperthermia and photodynamic therapy (PDT) has aroused interest. The combination has shown a supra-additive effect and has resulted in a greater depth of necrosis than obtained with either treatment modality applied alone (Waldow *et al* 1987, Mang 1990).

Because the cellular response to hyperthermia is highly dependent on the temperature (Dewey 1994), it is desirable to have complete knowledge of the temperature within both the treated tumour and the surrounding normal tissue. Currently, clinical thermometry during hyperthermia treatment relies on the use of invasive temperature probes such as micro-thermocouples and thermistors. Thus information regarding the tissue temperature is confined to a few points only, because the number of probes that can be implanted is limited by patient tolerance and practical clinical considerations.

A mathematical model can be used to extract the tissue temperature distribution from the invasive measurements. In this way, the treatment efficiency can be assessed more precisely. The temperature distribution can also be predicted by a mathematical model for accurate

0031-9155/95/122037+16$19.50

planning of hyperthermia treatment. Furthermore, a model can be used for extensive and inexpensive simulations of different heating configurations in order to optimize the treatment.

A number of mathematical models have been developed for predicting the thermal response during hyperthermia induced by microwaves (Chen *et al* 1990, Cherry and Iskander 1993, Dubois *et al* 1993, Moros *et al* 1993) and hot source implants (Babbs *et al* 1990, De Ford *et al* 1990, Haider *et al* 1993). Another way of inducing hyperthermia is to utilize the radiant energy from a laser. Several investigators have pointed out the potential of using a Nd:YAG laser to produce controlled heating in tissue, induced either by surface irradiation or, interstitially, using optical fibres (Daikuzono *et al* 1987, Mang 1990, Hahl *et al* 1990, Panjehpour *et al* 1991, Waldow *et al* 1992). An abundance of thermal models has been developed to describe the temperature distribution in laser-irradiated tissues (Halldorsson and Langerholc 1978, Welch and Polhamus 1984, Svaasand *et al* 1985, Jacques and Prahl 1987, Davis *et al* 1989, Whiting *et al* 1989, Grossweiner *et al* 1990, Sagi *et al* 1992, Torres *et al* 1993); for reviews, see Welch (1984) and McKenzie (1990). However, most previous thermal light–tissue models have only been verified for short irradiation times. In contrast, this study focuses on prolonged laser-induced heat treatment at a moderate temperature.

When modelling the thermal tissue response during surface-applied laser-induced hyperthermia, the heat exchange mechanisms at the tissue–air interface must be considered. With the exception of Torres *et al* (1993), previously published non-ablative models have not incorporated the heat loss due to surface evaporation of water. However, based on surface temperature measurements, Torres *et al* (1993) came to the conclusion that evaporation should be included in a model for the surface temperature if the surface temperature exceeded 60 °C In the present study, the thermal importance of surface evaporation for deep tissue at temperatures below 60 °C is investigated.

The thermal response of tissue to laser irradiation depends both on the optical and on the thermal properties of the tissue. Various models of light propagation in turbid media such as tissue have been proposed. One of the most common approaches has been the radiative transfer theory (Chandrasekhar 1960) providing the equation of radiative transfer. Since general solutions to the equation of radiative transfer are not available, various approximations, including the diffusion approximation (Ishimaru 1978) and the seven-flux model (Yoon *et al* 1987), have been proposed. Alternatively, the equation of radiative transfer can be solved numerically or the light fluence distribution can be simulated using the Monte Carlo method (Wilson and Adam 1983). The Monte Carlo method implies the trace following of a great number of single photons in the tissue, resulting in the distribution of absorbed photons. The advantage of this method in comparison with the above-mentioned methods lies in its ability to calculate the light transport even near light sources and boundaries with any required accuracy. Furthermore, the light absorption in tissues with a layered structure of different optical properties can be modelled straightforwardly. The subsequent heat propagation of the light energy can then be modelled by the heat-conduction equation (Carslaw and Jaeger 1989).

In this paper, a numerical model for calculating the temperature distribution in laser-irradiated tissue to be used in laser-induced hyperthermia is presented. The light distribution in surface-irradiated tissue is calculated from Monte Carlo simulations which then constitutes the source term in the heat conduction equation, which is solved numerically by an explicit finite-difference technique. Comparisons of the numerical results with *in vitro* experimental measurements on bovine liver were made in order to evaluate the effectiveness of the model. The model boundary condition at the laser-irradiated surface included the cooling mechanism of water evaporation. Using the model, the influence on the tissue temperature distribution of evaporation of water was examined theoretically for different blood perfusion rates. An

application of the model to temperature regulation during laser-induced hyperthermia was also investigated theoretically.

2. The mathematical model

The numerical model is based on the following bioheat-transfer equation:

$$\rho c \frac{\partial T}{\partial t} = \nabla(\lambda \nabla T) + Q_s + Q_p \tag{1}$$

where T is the temperature (K), ρ is the tissue density (kg m^{-3}), c is the specific heat of the tissue (J kg^{-1} K^{-1}) and λ is the thermal conductivity of the tissue (W m^{-1} K^{-1}). The time is represented by t (seconds), Q_s is the external heat-source term (W m^{-3}) and Q_p is the heat removal due to perfusion (W m^{-3}). Because the metabolic heat generation is generally much smaller than the external heat deposited (Jain 1983), this term has been omitted in the above expression.

The perfusion term was modelled according to Pennes (1948):

$$Q_p = -\omega \rho_b c_b \rho (T - T_a) \tag{2}$$

where ω is the blood perfusion rate ($m^3_{blood} s^{-1} kg^{-1}_{tissue}$), ρ_b is the density of blood (kg m^{-3}), c_b is the specific heat of blood (J kg^{-1} K^{-1}) and T_a is the local arterial temperature (K) which has frequently been assumed to be the body core temperature. This expression for the perfusion term neither accounts for the presence of major blood vessels nor deals with the directionality in the convective losses. However, it has been shown to give useful approximations of the general temperature distribution (Pennes 1948, Moros *et al* 1993) and is attractive due to the mathematical simplicity of the expression. For a survey of alternative models for perfusion, see Arkin *et al* (1994).

Equation (1) was solved using an explicit finite-difference technique based on the control volume formulation, assuming constant tissue thermal properties. As laser-light propagation in tissue is often well described in cylindrical symmetry, this representation was chosen. Thus, a cylindrical calculation domain was subdivided into a number of ring-shaped control volumes. A control volume of size $V_{i,j}$ (m^3) was identified by a single node at its centre (i, j) (figure 1).

By applying equation (1) to an internal control volume, namely a control volume not located at the upper surface, and using finite differences, the control volume temperature is given by:

$$\begin{aligned} T^{n+1}_{i,j} = T^n_{i,j} &- \omega \rho_b c_b \Delta t (T^n_{i,j} - T_a)/c_j + q_{i,j} \Delta t/(\rho_j c_j) \\ &- \Delta t[(T^n_{i,j} - T^n_{i,j-1})/(\delta z_j/\lambda_j + \delta z_{j-1}/\lambda_{j-1}) \\ &+ (T^n_{i,j} - T^n_{i,j+1})/(\delta z_j/\lambda_j + \delta z_{j+1}/\lambda_{j+1})]/(2\delta z_j \rho_j c_j) \\ &- 4\pi \lambda_j \delta z_j \Delta t[(T^n_{i,j} - T^n_{i-1,j})/\ln(r_i/r_{i-1}) \\ &+ (T^n_{i,j} - T^n_{i+1,j})/\ln(r_{i+1}/r_i)]/(\rho_j c_j V_{i,j}). \end{aligned} \tag{3}$$

The superscripts n and $n+1$ of the control volume temperatures represent successive time steps of size Δt. The subscripts of the density and the specific heat capacity indicate the possibility of defining a layered structure with different thermal properties. The absorbed laser power in the control volume is $q_{i,j}$(W m^{-3}). All geometric quantities in equation (3) are illustrated in figure 1.

The boundary conditions were chosen as follows. Due to the radial symmetry, no heat flows across the centre line, giving $\partial T/\partial r = 0$ at $r = 0$. The boundary conditions imposed

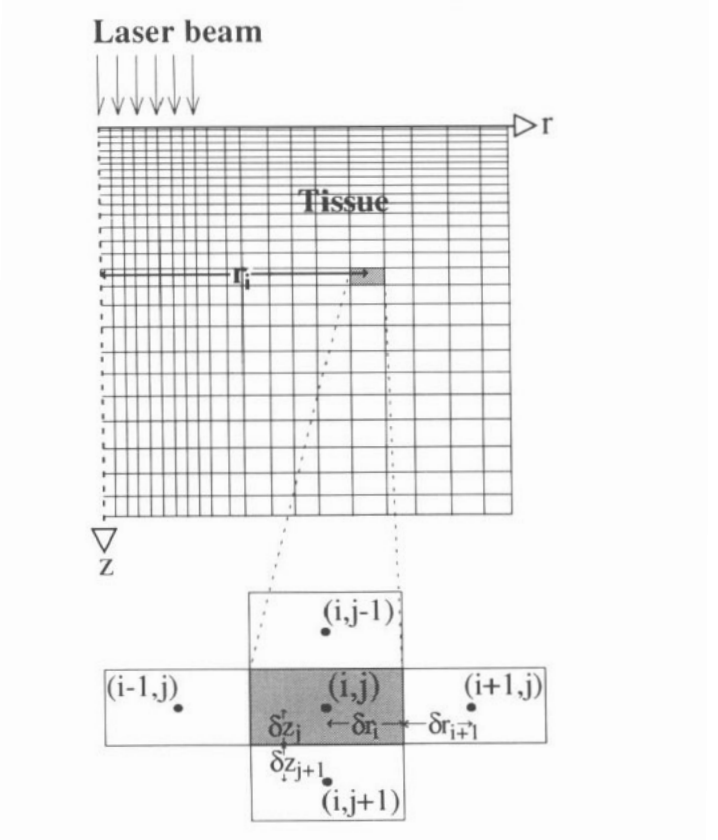

Figure 1. A schematic illustration of the two-dimensional model geometry in the general case In the model evaluation the special case of constant grid spacing was used.

on the lateral and bottom surface of the model cylinder, located far from the laser source, were $\partial T/\partial r = 0$ and $\partial T/\partial z = 0$ respectively, signifying isolated boundaries.

By convention, the surface boundary control volumes were modelled by placing the nodes on the upper surface of the control volumes instead of at the centres. The boundary condition at the upper laser-irradiated surface included heat loss from convection, radiation and evaporation. The surface boundary condition is mathematically described by

$$-\lambda\frac{\partial T}{\partial z} = h_c(T_e - T_s) + \sigma\varepsilon(T_e^4 - T_s^4) + q_e \qquad z = 0 \tag{4}$$

where h_c is the convective heat transfer coefficient (W m^{-2} K^{-1}), T_e and T_s are the environmental and surface temperatures (K), respectively, σ is the Stefan–Boltzmann constant equal to 5.696×10^{-8} W m^{-2} K^{-4} and ε is the emissivity (dimensionless). The heat flux due to evaporation is represented by q_e (W m^{-2}).

The convective heat transfer coefficient under free convection was calculated for a flat square plate using the following relationship (Sekins and Emery 1982):

$$h_c = 0.54k_f[g_{loc}\beta(T_s - T_e)\mathrm{Pr}/(D\nu^2)]^{0.25} \tag{5}$$

where k_f is the thermal conductivity of air equal to 2.62×10^{-2} W m^{-1} K^{-1} at a temperature of 300 K, g_{loc} is the local acceleration due to gravity taken to be 9.81 m s^{-2}, β is the volume coefficient of expansion of air (K^{-1}) evaluated as the inverted mean value of the surface

and environmental temperatures, Pr is the Prandtl number for air (dimensionless) equal to 0.708 at 300 K, D is a characteristic length (m) equal to the length of one side of the square plate and ν is the kinematic viscosity of air equal to 1.57×10^{-5} m^2 s^{-1} at 300 K. See Incropera and De Witt (1990) for full temperature-dependent values.

Evaporation of water from the laser-irradiated surface was modelled by the heat and mass transfer analogy for evaporation from a free water surface (Incropera and De Witt 1990):

$$q_e = h_{fg} h_m (\rho_{v,e} - \rho_{v,sat}) \tag{6}$$

where h_{fg} is the phase-change enthalpy of water at the surface temperature T_s, which at a surface temperature of 37 °C equals 2.41×10^6 J kg^{-1} (Sekins and Emery 1982), h_m is the convection mass transfer coefficient (m s^{-1}), $\rho_{v,e}$ is the density of water vapour in air (kg m^{-3}) at room temperature and $\rho_{v,sat}$ is the mass density of saturated water vapour (kg m^{-3}) at T_s. With a relative humidity of the ambient air of 30% at a temperature of 23 °C, $\rho_{v,e}$ equals 6.19×10^{-3} kg m^{-3}. The density of saturated water vapour is highly temperature-dependent, increasing from 20.6×10^{-3} to 51.2×10^{-3} kg m^{-3} between 23 and 40 °C. The convection mass transfer coefficient can be expressed as (Incropera and De Witt 1990)

$$h_m = h_c / (\rho_a c_a \mathrm{Le}^{2/3}) \tag{7}$$

where ρ_a and c_a are the density and specific heat of air, respectively, of which the product equals 1.18×10^3 J m^{-3} K^{-1} at 300 K and Le is the Lewis number (dimensionless) for the diffusion of water vapour into air, taken to be 0.865 (Incropera and De Witt 1990).

In the finite-difference formulation of equation (4), the total heat flux through the upper bounding surface into a surface control volume can now be modelled as

$$q_{surf(i,0)} = h_c (T_e - T_{i,0}) + \sigma \varepsilon (T_e^4 - T_{i,0}^4) + h_c h_{fg} (\rho_{v,e} - \rho_{v,sat}) / (\rho_a c_a \mathrm{Le}^{2/3}) \tag{8}$$

where $q_{surf(i,0)}$ is the total heat flux into a surface control volume represented by the node $(i,0)$. In the model, the convection heat transfer coefficient, h_c, was evaluated for all surface nodes at the temperature of the surface node adjacent to the axis of symmetry; that is at $T_{0,0}$. The characteristic length in equations (5) and (6) was chosen to be equal to the length of one side of the experimental liver samples. The density of saturated water vapour, $\rho_{v,sat}$, was evaluated at the local surface temperature $T_{i,0}$.

Stability is ensured by preventing the total energy content of a control volume from leaving the volume during the time step Δt. For the internal control volumes, this criterion is equivalent to a positive factor in front of the temperature T^n in equation (3), thereby limiting the maximum time step. For the surface nodes, with a more complex dependence on the temperature, the stability time step was calculated regarding a 'practical worst case'. At the temperatures and the sizes of the control volumes used in this investigation, the stability time step for the internal control volumes was found, in practice, to ensure stability in all control volumes.

The source terms in equation (3) were modelled by Monte Carlo simulations (Wang and Jacques 1992) for a tissue surface-irradiated at normal incidence with a chosen beam intensity profile. By defining the optical parameters of the tissue, μ_a (m^{-1}), μ_s (m^{-1}) and g (dimensionless), the Monte Carlo simulations give the light absorption probability (m^{-3}) in a two-dimensional, axially symmetric geometry, which provides a matrix of control volumes. The absorption probability multiplied by the total laser power then constituted the source terms, $q_{i,j}$, in equation (3).

3. Materials and methods

In vitro experiments were performed on samples of bovine liver in order to evaluate the validity of the model in predicting the temperature increase during laser-induced hyperthermia. Especially the thermal influence of water evaporation from the laser-irradiated surface was investigated. Measurements were performed on cubic samples of fresh bovine liver of approximately 4 cm side length. The liver samples were permitted to equilibrate at room temperature closely wrapped in thin plastic film to avoid water evaporation. The liver samples were then placed between two plates of PVC plastic. In figure 2, the experimental set-up is shown. Temperature measurements were made using thermistors (Yellow Springs Inc, Model 511) of 600 μm diameter, connected to an A/D converter and a PC. Individual calibration of the thermistors was performed prior to the experiments in a heated, well stirred water bath which was allowed to cool. The water temperature was measured with a mercury-in-glass thermometer of accuracy ± 0.1 °C. Calibration readings were taken every 0.5 °C in the interval 18–60 °C. The temperature in the experimental measurements was then given by linear interpolation between the calibration points.

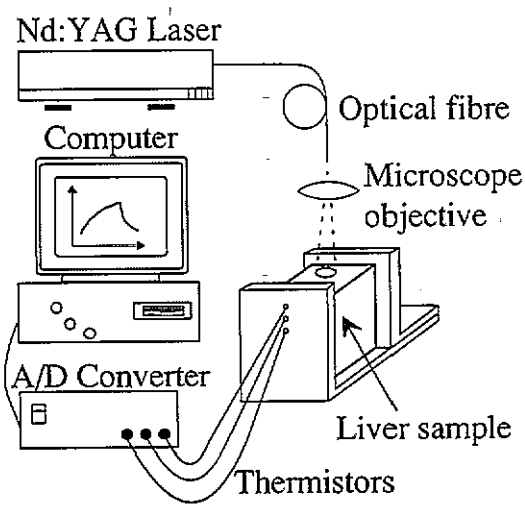

Figure 2. The experimental set-up for the *in vitro* experiments on bovine liver. The upper liver surface was either covered with thin plastic film or moistened with water.

The thermistors were inserted horizontally into the tissue, using hollow needles, through drilled holes in one plastic plate. The thermistors were located on a common vertical axis at three different depths (3.5, 6.5 and 9.5 mm) and the needles were withdrawn. An expanded beam from a Nd:YAG laser (Quantronix 116 SFW0/CW) emitting at 1064 nm was used to irradiate the tissue from above. The beam from a 600 μm diameter fibre was expanded by a microscope objective to generate a 'top hat' intensity distribution on the liver surface. In figure 3, the measured intensity distribution over two diameters of the spot is shown, indicating uniform spot intensity. The intensity distribution was obtained by traversing the spot with a 400 μm diameter optical fibre while measuring the intensity every 0.5 mm.

The beam spot size on the tissue surface was adjusted to 2.0 cm with its centre above the thermistors as determined from the insertion length of the withdrawn needles. The total beam power was set to 1.6 W, measured with an Astral power meter (Scientech, Model AA 30), resulting in an incident fluence rate of 510 mW cm^{-2}. The tissue surface was irradiated for 15 min during which the temperature was measured every other second. After 20 min,

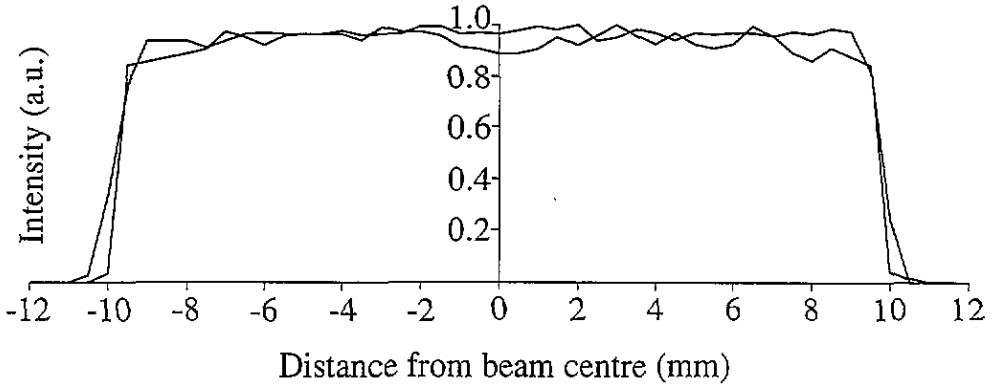

Figure 3. The measured intensity distribution over the laser beam spot expanded by a microscope objective, showing the spot intensity measured over two perpendicular diameters.

the measurements were terminated.

The influence on the tissue temperature of the surface evaporation of water was investigated by performing two series of experiments. In the first series, the liver surface was covered with thin plastic film to prevent surface evaporation of water. The transmission of the plastic film at 1064 nm was 94%, which was accounted for in the numerical simulations. In the second series, liver samples were irradiated without surface-covering plastic film. Immediately before the irradiation of the samples without the plastic film, the liver surface was moistened with water. The water had equilibrated at room temperature in a closed container to avoid evaporative cooling. The addition of water was motivated by the observation that, without the moisture, the liver surface tended to dry out by the end of the experiment, complicating the comparison with the numerical calculations. Five temperature measurements were performed at each of the three measurement points in each series of experiments.

The experimental results were compared with numerical simulations of an experimentally equivalent situation. In the model, the tissue geometry was chosen to be approximately equal to the liver sample size. Because the experimental measurement points used in the comparison with the numerical simulations were located close to the upper surface, the model geometry chosen was in practice a semi-infinite medium. The grid size used in the numerical simulations was $\delta r = \delta z = 0.25$ mm.

The thermal properties of the tissue were given by the following relationships (Welch 1984): $c = 4.19(0.37 + 0.63W) \times 10^3$ J kg^{-1} K^{-1} and $\lambda = 4.19(0.133 + 1.36W) \times 10^{-1}$ W m^{-1} K^{-1}, where W is the water mass content of the tissue. By assuming a dry liver tissue density of 1.3×10^3 kg m^{-3}, the liver tissue density was estimated from $\rho = (1.3 - 0.3W) \times 10^3$ kg m^{-3} (Jacques and Prahl 1987). The water mass content of bovine liver was measured by slowly oven-drying small tissue samples and was found to be 69%. Using the above relationships, the thermal properties of bovine liver were found to be $\rho = 1.09 \times 10^3$ kg m^{-3}, $\lambda = 0.45$ W m^{-1} K^{-1} and $c = 3.37 \times 10^3$ J kg^{-1} K^{-1}. The value of the emissivity, ε, used was 0.98, which value is representative of skin (Chato 1990). The environmental temperature was 23 °C and the characteristic length in equation (5) was set to 0.04 m. For the temperature-dependent factors in the evaporation term, tabulated values were used (Incropera and De Witt 1990).

The optical properties of the liver samples were taken to be $\mu_a = 0.5$ cm^{-1}, $\mu_s = 80.0$ cm^{-1} and $g = 0.97$, obtained at 1064 nm for porcine liver (Roggan *et al* 1993). The

refractive index of tissue was taken to be 1.38 (Jacques and Prahl 1987). The Monte Carlo simulations based on the above-defined optical parameters provided the light absorption distribution in the tissue for an irradiating beam with a 'top hat' intensity distribution.

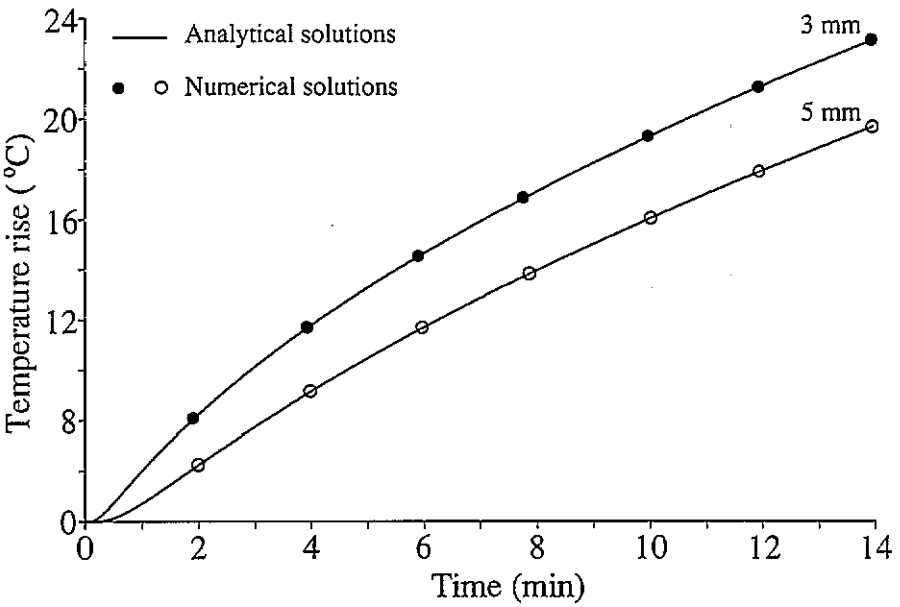

Figure 4. The numerical and analytical solutions for the temperature rise at depths of 3 and 5 mm in a semi-infinite tissue-like medium with a heat flux of 200 mW cm^{-2} through the upper surface.

In the numerical simulations of the experiments with the plastic film covering the liver surface, the surface evaporation term was excluded. The evaporation term was included in the simulations of the experiments without the plastic film, in which the surface had been moistened with water.

4. Results

The computer code developed was thoroughly tested by comparing the numerical simulation results with analytical solutions. The result of one of the tests performed is presented below.

Considering a constant heat flux, F_0, through the boundary to a semi-infinite medium having a constant initial temperature of T_0, the analytical solution of the temperature distribution is given by Carslaw and Jaeger (1989). The numerical results for the corresponding situation were obtained for a cylinder of 5 cm height and diameter. For the observed points and time of observation, the model cylinder can be assumed to be semi-infinite. The parameters chosen were $F_0 = 200$ mW cm^{-2}, $T_0 = 37\,^{\circ}C$, $\lambda = 0.45$ W m^{-1} K^{-1}, $c = 3.37$ J kg^{-1} K^{-1} and $\rho = 1.09$ kg m^{-3}. The surface heat processes (convection, radiation and evaporation) were neglected. Figure 4 shows the analytical and numerical solutions for the situation described above at depths of 3 and 5 mm, indicating the accuracy of the code.

Experiments on bovine liver were performed to evaluate the validity of the model for biological tissue. Figure 5 shows the averaged measured and calculated temperatures on the axis of symmetry at three different depths (3.5, 6.5 and 9.5 mm) as a function of time.

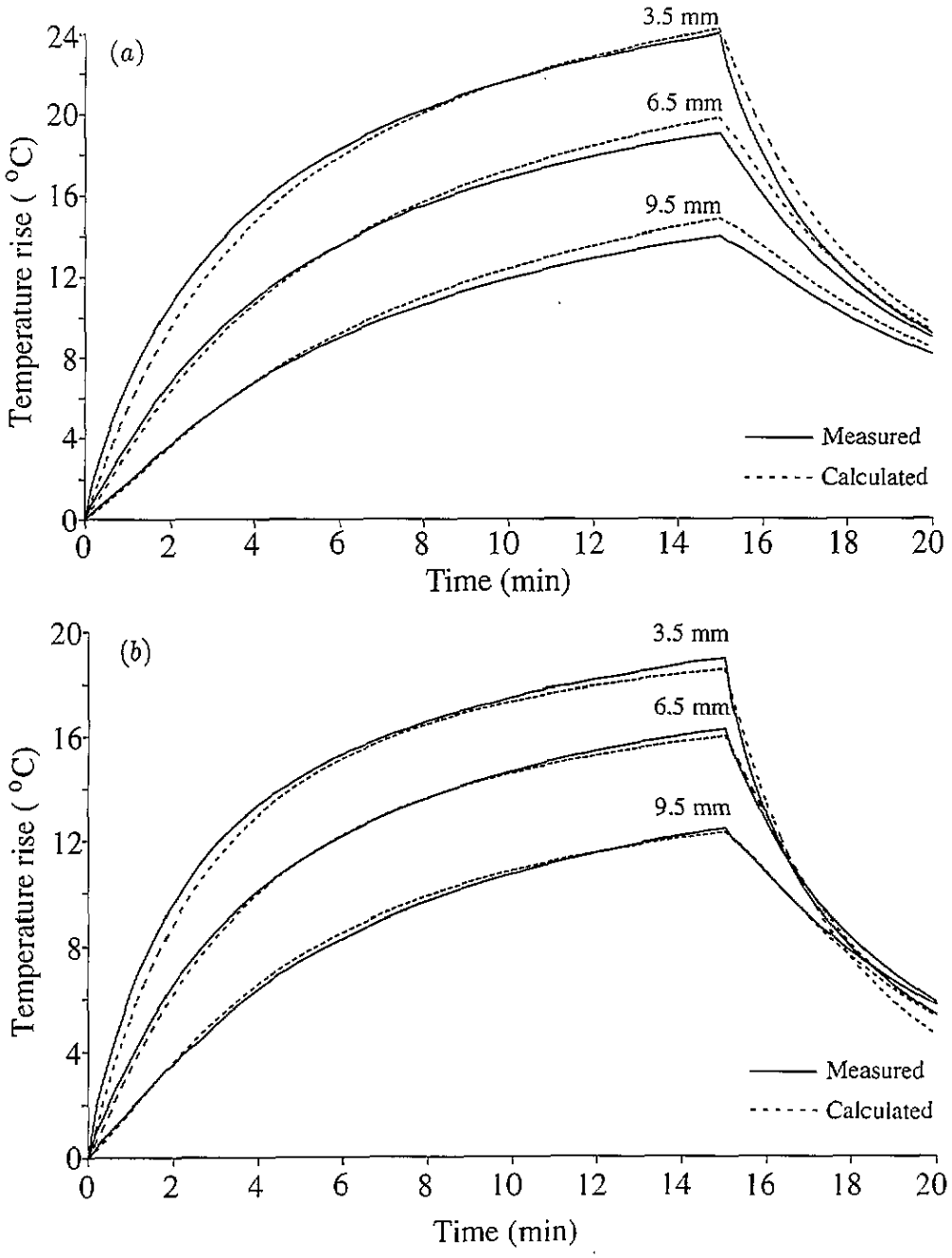

Figure 5. Averaged experimental (full lines) and numerical (broken lines) results for the temperature increase in the bovine liver samples at three different depths on the axis of symmetry of the irradiating beam. The samples were irradiated with 1.6 W at 1064 nm with a spot of 20 mm diameter. After 15 min, the laser was switched off. (*a*) The surface was covered with thin plastic film to prevent evaporation of water. In the numerical calculations, the surface boundary condition included only convection and radiation. (*b*) The surface-covering plastic film was removed and the surface was moistened with water prior to the experiments. In the numerical calculations, the surface evaporation term was included to account for evaporation.

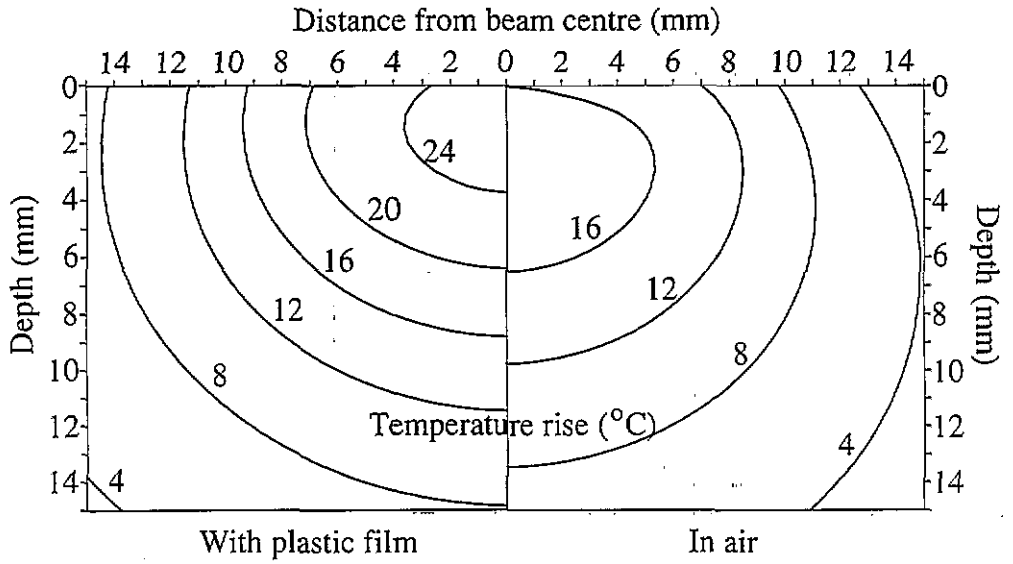

Figure 6. Calculated total temperature distributions after 15 min of irradiation. The irradiated spot diameter was 20 mm and the total beam power was 1.6 W. The temperature increase is shown with only convection and radiation considered at the surface (left) and with surface evaporation of water included (right). Because the temperature distributions are radially symmetric, only half of each distribution is shown.

Figure 5(*a*) shows results from the liver samples covered with thin plastic film. Figure 5(*b*) shows results from the samples irradiated in air with a moistened surface. Five experiments were performed at each measurement point. The laser was turned on at time $t = 0$ s and was switched off at $t = 900$ s (15 min). After 20 min, the measurements were terminated. The maximum standard deviation observed at the end of the laser irradiation was in all cases less than 1.2 °C. Student's t-test statistical evaluation applied to the experimental results showed a significantly greater temperature ($P < 0.01$) of the liver covered with plastic film after 3 min of irradiation at 3.5 mm depth. The irradiation times required to reach the corresponding significant temperature differences at 6.5 and 9.5 mm were 8 and 15 min, respectively. Figure 5 shows that there is a good fit between experimental and calculated temperatures, and that the process of surface evaporation is adequately described by the heat and mass transfer analogy.

The calculated temperature distributions after 15 min of irradiation with and without surface evaporation can be seen in figure 6. Because the temperature distribution is radially symmetric, only half of each distribution is shown. To indicate the relative importance of the different surface heat exchange mechanisms after 15 min of irradiation when allowing for evaporation, the heat losses due to convection, radiation and evaporation were calculated to be 100, 100 and 590 W m^{-2}, respectively, at a calculated surface temperature of 39 °C. The heat convection coefficient, h_c, was in this case equal to 6.2 W m^{-2} K^{-1}.

In hyperthermia therapy in the classical sense, the goal is to treat the tumour tissue at a homogeneous cytotoxic temperature, generally assumed to be above 43 °C, without any overheating of the surrounding tissue. The model developed here was used to investigate the influence of water evaporation at the surface on the total temperature distribution and the magnitude of the inevitable temperature gradients produced by the laser irradiation. Simulations were carried out for liver tissue with previously defined optical and thermal

properties. The liver was irradiated with a 2.0 cm diameter beam. Whenever the temperature at a depth of 10 mm exceeded 43 °C, the laser was switched off. After transient fluctuations, this simple regulation every 1.0 s prevented the temperature from fluctuating by more than 0.2 °C within the overlying volume. Figure 7 shows the temperature distribution at steady state (after 10 min) in the surface-irradiated liver in which the temperature at a depth of 10 mm was maintained at 43 °C. The left-hand side of figure 7(*a*) shows the temperature distribution without any blood flow present. The right-hand side shows the temperature distribution in liver tissue with a perfusion rate of $\omega = 9.61 \times 10^{-6}$ m^3_{blood} s^{-1} kg^{-1}_{tissue}, which is representative of human liver arterial perfusion (Sekins and Emery 1982). The heat capacity and density of blood were set to 3.64×10^3 J kg^{-1} K^{-1} and 1.05×10^3 kg m^{-3}, respectively (Sekins and Emery 1982) and the arterial temperature, T_a, was set to 37 °C. The initial liver temperature was set to 37 °C and surface evaporation was excluded. Figure 7(*b*) shows the corresponding situation in which surface evaporation was incorporated into the model. Figure 7(*c*) shows the temperatures on the axis of symmetry for the above-described situations at steady-state. The influence of the surface evaporation is seen in the significantly decreased surface temperature, forcing the maximum temperature to a greater depth.

The transient thermal response to the simulated laser-irradiation without any tissue perfusion is seen in figure 8, in which two regulation mechanisms are described. The broken lines represent the regulation in which the laser with 3.0 W total output power was turned on and off guided only by the temperature at a depth of 10 mm. The full lines represent the regulation whereby, in addition to the above-described condition, the maximum tissue temperature occurring at a depth of 4 mm was restricted so as not to exceed 46 °C. With the latter temperature regulation, the small temperature ripple at steady-state and the transient temperature build-up time at 10 mm were seen to be almost independent of the laser output power as soon as a lower threshold value of the laser power was exceeded (results not shown).

5. Discussion

In this paper, a numerical model for calculating the temperature distribution in surface-applied laser-induced hyperthermia is presented. The source terms in the equation of heat transfer were calculated based on Monte Carlo simulations for the light absorption distribution. The heat transfer equation was then solved using finite differences. Both the Monte Carlo and the heat transfer model allow the definition of a layered structure which could be used to simulate the heat transfer in laser-irradiated skin, for example. The model takes into account any axi-symmetric beam profile and calculates the temperature distribution in cylindrical coordinates. Surface irradiation was considered because this irradiation modality is frequently used in photodynamic therapy (PDT). The model developed is thus well suited for planning and evaluating hyperthermia treatment in conjunction with PDT.

The validity of the model was verified by comparisons of model simulations with analytical results and *in vitro* measurements on liver tissue. Very good agreement with analytical results was found. The calculated temperatures showed good agreement with the experimental results for liver tissue. The experimental temperature rise was predicted within 5% by the model after 15 min of irradiation. The degree of accuracy was the same whether surface evaporation of water was prevented by covering with a thin plastic film or allowed by removing the plastic film. In the model, the two cases corresponded to the exclusion and incorporation of the surface evaporation term, respectively. When irradiating in air and not accounting for surface evaporation in the model, the accuracy of the predictions was only 75–80%. The numerical simulations of the experiments showed that, at a surface

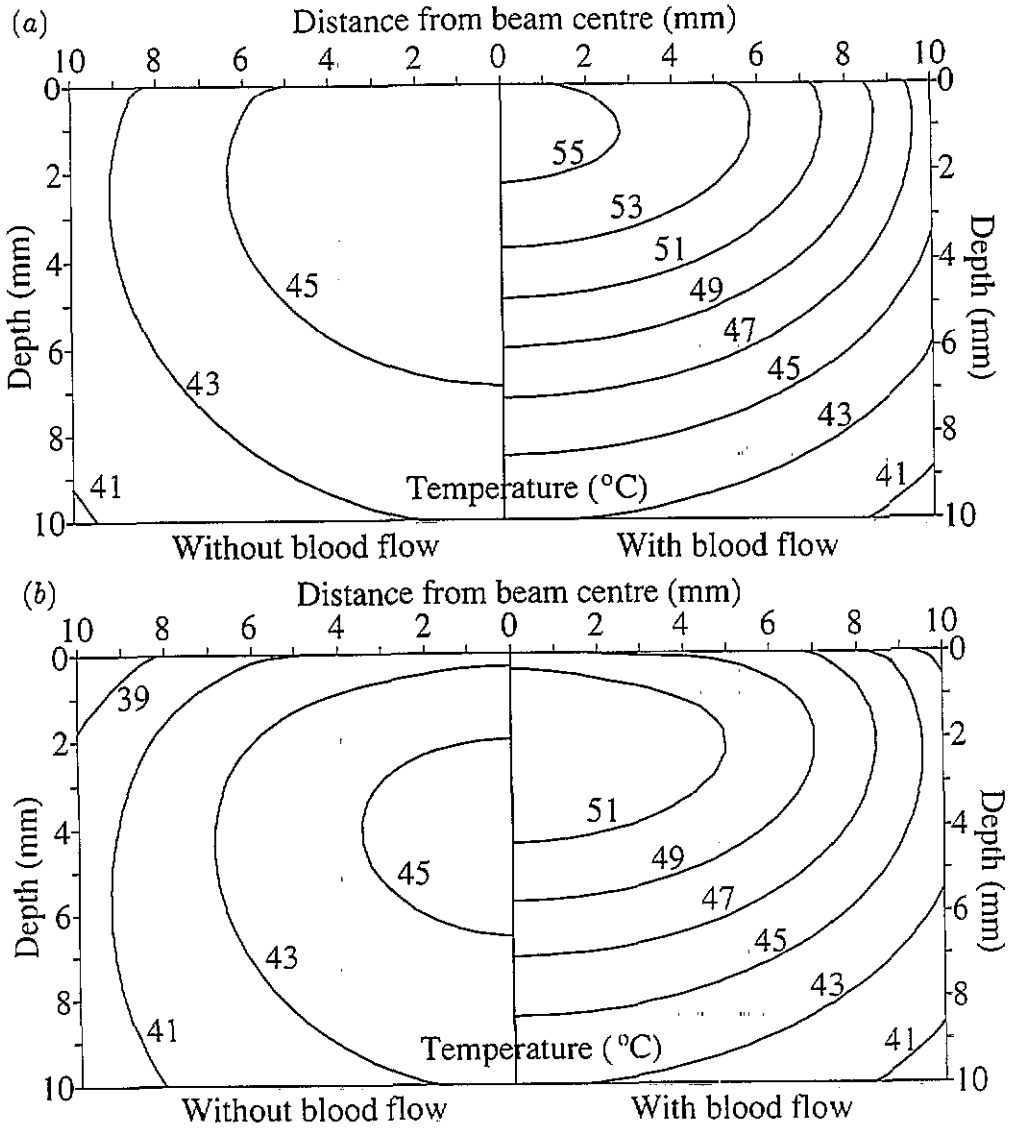

Figure 7. The calculated steady-state temperature distribution in a surface-irradiated liver in which the temperature at a depth of 10 mm on the axis of symmetry of the irradiating beam of 20 mm diameter was maintained at 43 °C. (*a*) The left-hand side shows values calculated without any blood flow. A blood flow rate corresponding to the human arterial liver blood flow was used in the calculations shown in the right-hand side temperature distribution. Only convection and radiation were considered at the upper surface. (*b*) The corresponding situation, except that surface evaporation of water was incorporated into the calculations. Because the temperature distributions are radially symmetric, only half of each distribution is shown. (*c*) The steady-state temperatures on the axis of symmetry of the irradiating beam.

temperature of 39 °C, the calculated heat loss due to evaporation was six times as important as the heat losses due to convection or radiation.

In the numerical calculations, the optical properties of porcine liver were used (Roggan *et al* 1993) due to the lack of values for all three (μ_s, μ_a and g) of these properties for bovine liver. For bovine liver, Karagiannes *et al* (1989) have reported only the absorption

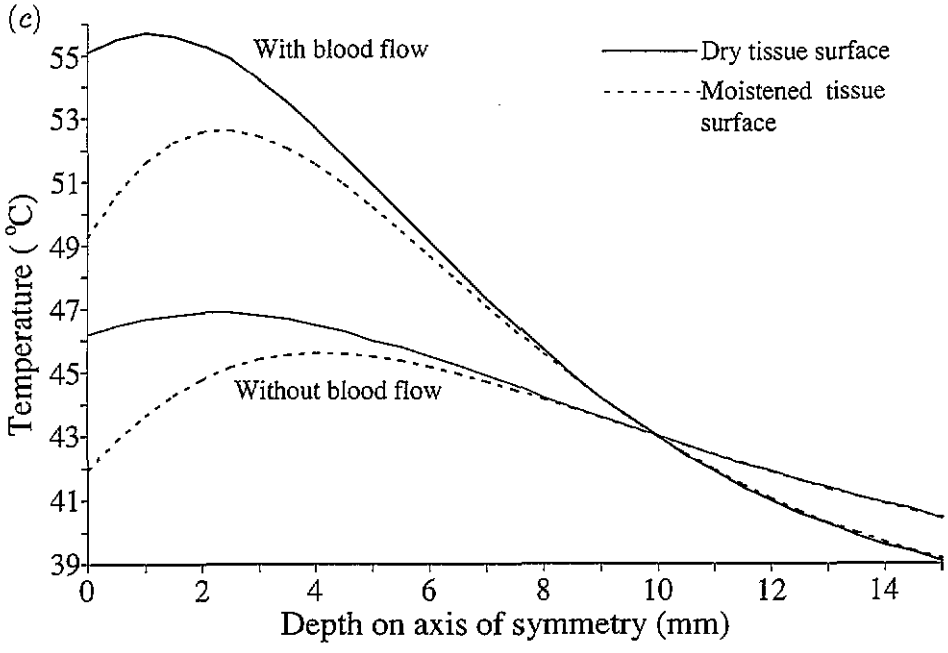

Figure 7. (Continued)

coefficient and reduced scattering coefficient, $\mu_s' = \mu_s(1-g)$. However, the absorption and reduced scattering coefficient provided by Roggan *et al* (1993) correspond well with the values reported by Karagiannes *et al* (1989) for bovine liver, justifying the use of the optical properties of porcine liver in the simulations.

To date, not many investigators have addressed the importance of water evaporation regarding the temperature of the irradiated tissue. However, in a study performed by Torres *et al* (1993), the evaporation of water was shown to be relevant for the surface temperature at surface temperatures above 60 °C and short irradiation times. In the present study, the influence of the evaporation on the deep tissue temperature was investigated. The simulations presented showed that evaporation of water is by far the most important heat loss mechanism compared with convection and radiation, even at temperatures as low as 39 °C. In laser-induced hyperthermia, the degree of wetness of the tissue surface could have implications for the calculated outcome of the treatment because the biological response of the tissue is highly dependent on the temperature (Dewey 1994): The importance of surface evaporation on the deep tissue temperature was exemplified by the numerically simulated temperature distributions in figure 7, in which the temperature at a depth of 10 mm was kept constant (43 °C). In the simulations including surface evaporation, the maximum tissue temperature was lowered and forced to a greater depth compared with the case when no evaporation was considered. The most significant influence on the tissue temperature was naturally at the surface, at which the temperature was lowered 4–6 °C depending on the blood flow rate. This would have implications on the estimation of the treatment depth using the thermal model based on surface temperature measurements. The calculated maximum temperature was forced to a depth of 4 mm for the tissue with a moistened surface and no blood flow. In conjunction with PDT, a moistened tissue surface thus allows the optimal thermal treatment to be applied at a depth at which the true synergism of PDT and hyperthermia is likely to occur (Mang 1990).

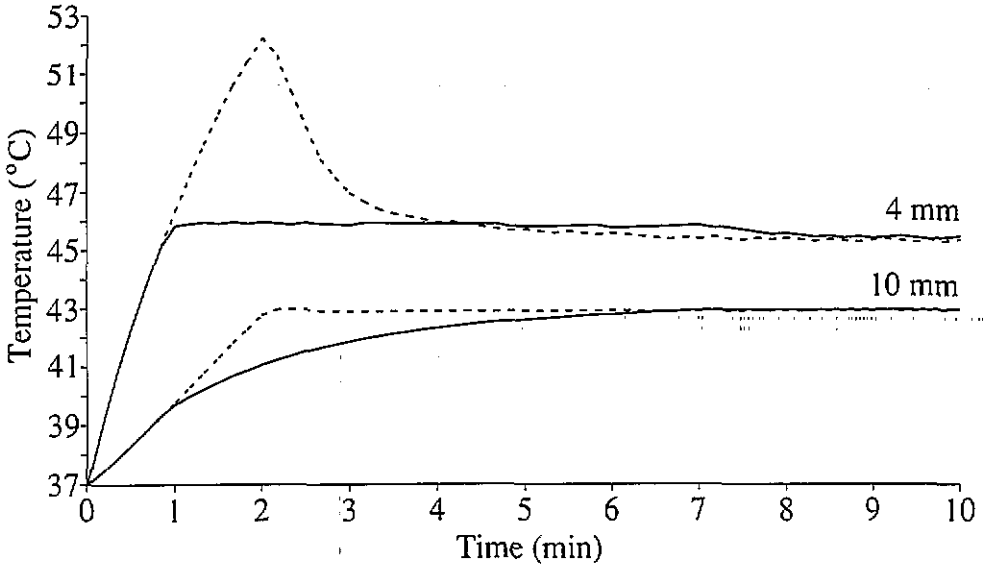

Figure 8. Numerical simulations showing how the thermal model can be used to prevent substantial overheating of the tissue during the thermal build-up time. The calculated temperatures at two different depths on the axis of symmetry of the 20 mm diameter irradiating beam are shown. The steady-state temperature at a depth of 10 mm was pre-set to attain a temperature of 43 °C. The broken lines represent the situation in which the laser irradiation was regulated only by the temperature at 10 mm. The full lines represent the situation in which the maximum tissue temperature also was restricted so as not to exceed 46 °C. No blood flow was considered.

Some sort of regulation of the tissue temperature in order to reach and maintain a desired level is indispensable in hyperthermia. This has been achieved by continuously varying the laser power guided by a master temperature probe placed in the tissue (Waldow *et al* 1992). However, for many laser systems, especially if the laser is not used exclusively for hyperthermia treatment, this type of regulation may be practically unsuitable because it may require some kind of laser modification. Therefore, a more simple form of regulation using an external shutter was investigated with the model. It was found that, by using a shutter regulated every second, it was theoretically possible to control the temperature at a depth of 10 mm without producing any significant temperature fluctuations in the overlying volume. Similar results have previously been reported from experimental studies (Panjehpour *et al* 1991). However, in contrast to that study, the present numerical simulations did not show any large temperature variations at the surface. This may possibly be explained by the smaller size of the irradiating spot used by Panjehpour *et al* (1991).

When the shutter was regulated by a pre-set maximum temperature within the tissue together with the temperature at a depth of 10 mm, the transient overheating of the tissue was avoided, as can be seen in figure 8. For regulation purposes, the model can thus be used to simulate the first part of hyperthermia treatment to avoid any unnecessary overheating of the tissue. With a suitable set of thermal and optical parameters for tissue and an estimation of the blood perfusion, simulations can be performed for the transient temperature build-up time. During the initial phase of the hyperthermia treatment, the simulations can control the shutter so that the maximum temperature in the tissue does not rise excessively, as indicated in figure 8. After a certain time, a master temperature probe within the tissue can be given control of the shutter to establish steady-state. The numerical simulations also

demonstrated that by using the two-point shutter regulation the transient and steady-state tissue temperatures were insensitive to the laser power chosen (not shown). Alternatively, for this kind of regulation, a temperature probe implanted at the expected location of the maximum temperature can be used. However, temperature measurements close to the irradiated surface may prove to be inaccurate due to direct laser-light absorption by the probe.

6. Conclusion

It has been shown that the temperature rise in liver tissue, laser-irradiated at the surface, can be modelled with 5% accuracy. By successful incorporation into the model of water evaporation at the surface, the 5% accuracy was found to apply both to the plastic-film covered samples and to the samples in air allowing surface evaporation. By moistening the liver surface, it was shown theoretically that the surface temperature was substantially lowered and that the maximum temperature could be forced into the tissue to a depth of 4 mm. An application of the model to temperature regulation was also presented, suggesting that the use of a shutter in controlling the amount of laser irradiation is sufficient to attain a steady temperature. By using the model for temperature regulation during hyperthermia treatment, it was shown that overheating of the tissue could be prevented.

Acknowledgments

The support of Professor S Svanberg is gratefully acknowledged. This work was financially supported by the Swedish Natural Science Research Council and the Swedish Research Council of Engineering Sciences.

References

Arkin H, Xu L X and Holmes K R 1994 Recent developments in modeling heat transfer in blood perfused tissues *IEEE Trans. Biomed. Eng.* **41** 97–107

Babbs C F, Fearnot N E, Marchosky J A, Moran C J, Jones J T and Plantenga T D 1990 Theoretical basis for controlling minimal tumor temperature during interstitial conductive heat therapy *IEEE Trans. Biomed. Eng.* **37** 662–72

Carslaw H S and Jaeger J C 1989 *Conduction of Heat in Solids* 2nd edn (Oxford: Clarendon)

Chandrasekar S 1960 *Radiative Transfer* (Oxford: Oxford University Press)

Chato J C 1990 Fundamentals of bioheat transfer *Thermal Dosimetry and Treatment Planning* ed M Gautherie (Berlin: Springer) pp 1–56

Chen Z P, Miller W H, Roemer R B and Cetas T C 1990 Errors between two- and three-dimensional thermal model predictions of hyperthermia treatments *Int. J. Hyperthermia* **6** 175–91

Cherry P C and Iskander M F 1993 Calculations of heating patternas of an array of microwave interstitial antennas *IEEE Trans. Biomed. Eng.* **40** 771–9

Daikuzono N, Joffe S N, Tajiri H, Suzuki S, Tsunekawa H and Ohyama M 1987 Laserthermia: a computer-controlled contact Nd:YAG system for interstitial local hyperthermia *Med. Instrum.* **21** 275–7

Davis M, Dowden J, Steger A, Kapadia P and Whiting P 1989 A mathematical model for interstitial laser treatment of tumours using four fibers *Lasers Med. Sci.* **4** 41–53

De Ford J A, Babbs C F, Patel U H, Fearnot N E, Marchosky J A and Moran C J 1990 Accuracy and precision of computer-simulated tissue temperatures in individual human intracranial tumours treated with interstitial hyperthermia *Int. J. Hyperthermia* **6** 755–70

Dewey W C 1994 Arrhenius relationships from the molecule and cell to the clinic *Int. J. Hyperthermia* **10** 457–83

Dubois L, Pribetich J, Fabre J-J, Chive M and Moschetto Y 1993 Non-invasive microwave multifrequency radiometry used in microwave hyperthermia for bidimensional reconstruction of temperature patterns *Int. J. Hyperthermia* **9** 415–31

Grossweiner L I, Al-Karmi A M, Johnson P W and Brader K R 1990 Modeling of tissue heating with a pulsed Nd:YAG laser *Lasers Surg. Med.* **10** 295–302

Hahl J, Haapiainen R, Ovaska J, Puolakkainen P and Schröder T 1990 Laser-induced hyperthermia in the treatment of liver tumors *Lasers Surg. Med.* **10** 319–21

Haider S A, Cetas T C and Roemer R B 1993 Temperature distribution in tissues from a regular array of hot source implants: an analytical approximation *IEEE Trans. Biomed. Eng.* **40** 408–17

Halldorsson T and Langerholc J 1978 Thermodynamic analysis of laser irradiation of biological tissue *Appl. Opt.* **17** 3948–58

Incropera F P and De Witt D P 1990 *Fundamentals of Heat and Mass Transfer* 3rd edn (New York: Wiley)

Ishimaru A 1978 *Wave Propagation and Scattering in Random Media* (New York: Academic)

Jacques S L and Prahl S A 1987 Modeling optical and thermal distribution in tissue during laser irradiation *Lasers Surg. Med.* **6** 494–503

Jain R K 1983 Bioheat transfer: mathematical models of thermal systems *Hyperthermia in Cancer Therapy* ed F K Storm (Boston: Hall) pp 9–46

Karagiannes J L, Zhang Z, Grossweiner B and Grossweiner L 1989 Applications of the 1-D diffusion approximation to the optics of tissues and tissue phantoms *Appl. Opt.* **12** 2311–17

Mang T S 1990 Combination studies of hyperthermia induced by the neodymium : yttrium-aluminum-garnet (Nd:YAG) laser as an adjuvant to photodynamic therapy *Lasers Surg. Med.* **10** 173–8

McKenzie A L 1990 Physics of thermal processes in laser-tissue interaction *Phys. Med. Biol.* **35** 1175–209

Molls M 1992 Hyperthermia—the actual role in radiation oncology and future prospects. Part I *Strahlenther. Onkol.* **168** 183–90

Moros E G, Dutton A W, Roemer R B, Burton M and Hynynen K 1993 Experimental evaluation of two simple thermal models using hyperthermia in muscle *in vivo Int. J. Hyperthermia* **9** 581–98

Overgaard J 1989 The current and potential role of hyperthermia in radiotherapy *Int. J. Radiat. Oncol. Biol. Phys.* **16** 535–49

Panjehpour M, Wilke A V, Frazier D L and Overholt B F 1991 Nd:YAG laser hyperthermia treatment of rat mammary adenocarcinoma in conjunction with surface cooling *Lasers Surg. Med.* **11** 356–62

Pennes H H 1948 Analysis of tissue and arterial blood temperatures in the resting human forearm *J. Appl. Physiol.* **1** 93–122

Roggan A, Minet O, Schröder C and Müller G 1993 Measurements of optical properties of tissue using integrating sphere technique *SPIE Inst. Med. Opt. Tomography* **11** 149–65

Sagi A, Shitzer A, Katzir A and Akselrod S 1992 Heating of biological tissue by laser irradiation: theoretical model *Opt. Eng.* **31** 1417–24

Seegenschmiedt H J, Feldmann H J and Molls M 1993 Hyperthermia—the actual role in radiation oncology and future prospects. Part II: clinical fundamentals and results in superficial tumors *Strahlenther. Onkol.* **169** 635–54

Sekins K M and Emery A F 1982 Thermal science for physical medicine *Therapeutic Heat and Cold* ed J F Lehmann (Baltimore, MD: Williams and Wilkins) pp 70–132

Svaasand L O, Boerslid T and Oeveraasen M 1985 Thermal and optical properties of living tissue: application to laser-induced hyperthermia *Lasers Surg. Med.* **5** 589–602

Torres J H, Motamedi M, Pearce J A and Welch A J 1993 Experimental evaluation of mathematical models for predicting the thermal response of tissue to laser irradiation *Appl. Opt.* **32** 597–606

Waldow S M, Henderson B W and Dougherty T J 1987 Hyperthermic potentiation of photodynamic therapy employing Photofrin I and II: comparison of results using three animal tumor models *Lasers Surg. Med.* **7** 12–22

Waldow S M, Russel G E and Wallner P E 1992 Microprocessor-controlled Nd:YAG laser for hyperthermia induction in the RIF-1 tumor *Lasers Surg. Med.* **12** 417–24

Wang L and Jacques S L 1992 *Monte Carlo Modeling of Light Transport in Multi-layered Tissues in Standard C* (Houston, TX: M D Anderson Cancer Center)

Welch A J 1984 The thermal response of laser irradiated tissue *IEEE J. Quant. Electron.* **20** 1471–81

Welch A J and Polhamus G D 1984 Measurement and prediction of thermal injury in the retina of the rhesus monkey *IEEE Trans. Biomed. Eng.* **31** 633–44

Whiting P, Dowden J and Kapadia P 1989 A mathematical analysis of the results of experiments on rats' livers by local laser hyperthermia *Lasers Med. Sci.* **4** 55–64

Wilson B C and Adam G 1983 A Monte Carlo model for the absorption and flux distributions of light in tissue *Med. Phys.* **10** 824–30

Yoon G, Welch A J, Motamedi M and van Gemert M J C 1987 Development and application of three-dimensional light distribution model for laser irradiated tissue *IEEE J. Quant. Electron.* **23** 1721–33